Ann. Naturhist. Mus. Wien, Serie A	113	35–65	Wien, Mai 2011

A new expanded record of the Paleocene-Eocene transition in the Gosau Group of Gams (Eastern Alps, Austria)

By Michael Wagreich[1], Hans Egger[2], Holger Gebhardt[2], Omar Mohammed[3,4], Christoph Spötl[5], Veronika Koukal[1] and Gerhard Hobiger[2]

(With 2 plates, 9 figures and 3 tables)

Manuscript submitted on October 14th 2010,
the revised manuscript on March 3rd 2011

Abstract

A Paleocene/Eocene-boundary section is described from the Zwieselalm Formation of the Upper Gosau Subgroup at Gams, Northern Calcareous Alps, Austria. The Pichler section exposes 122 m of turbidite-dominated psammitic to pelitic deposits. Occasionally, thin layers and concretions occur consisting essentially of early diagenetic siderite. The Paleocene/Eocene- boundary at the base of the Pichler section is characterized by a negative excursion of carbon isotope values (CIE), the occurrences of the dinoflagellate cyst *Apectodinium augustum* and the calcareous nannoplankton species *Discoaster araneus* and *Rhomboaster* spp. Foraminiferal assemblages are predominantly allochthonous and indicate deposition below the calcite compensation depth in the lower to middle part of the section. High sedimentation rates of ca. 20 cm/kyr are estimated.

Keywords: Paleocene/Eocene-boundary, Northern Calcareous Alps, turbidites, calcareous nannoplankton, foraminifera

Zusammenfassung

Ein Paleozän/Eozän-Grenzprofil wird aus der Zwieselalm-Formation der Oberen Gosau-Subgruppe der Nördlichen Kalkalpen (Österreich) beschrieben. Das Pichler-Profil erschließt 122 m einer von Turbiditen dominierten sandig-pelitischen Abfolge. Gelegentlich sind dünne Lagen mit

[1] Universität Wien, Department für Geodynamik und Sedimentologie, Althanstraße 14, 1090 Wien, Austria; e-mail: michael.wagreich@univie.ac.at, vkoukal@hotmail.com
[2] Geologische Bundesanstalt, Neulinggasse 38, 1030 Wien, Austria; e-mail: johann.egger@geologie.ac.at, holger.gebhardt@univie.ac.at
[3] Universität Graz, Institut für Erdwissenschaften (Geologie und Paläontologie), Heinrichstrasse 26, 8010 Graz, Austria; e-mail: omaraosman@yahoo.com
[4] El-Minia University, Faculty of Science, Geology Department, El-Minia, Egypt.
[5] Universität Innsbruck, Institut für Geologie und Paläontologie, Innrain 52, 6020 Innsbruck, Austria; e-mail : christoph.spoetl@uibk.ac.at

Konkretionen vorhanden, die vor allem aus frühdiagenetischem Siderit bestehen. Die Paleozän/Eozän-Grenze ist gekennzeichnet durch eine negative Anomalie der Kohlenstoff-Isotopenwerte, das Auftreten der Dinoflagellatenart *Apectodinium augustum* und dem Erstauftreten der kalkigen Nannoplanktonarten *Discoaster araneus* und *Rhomboaster* ssp. Foraminiferenvergesellschaftungen sind vorwiegend allochthon und weisen auf eine Ablagerung unter der Kalzitkompensationstiefe im unteren und mittleren Abschnitt des Profils hin. Hohe Sedimentationsraten von ca. 20 cm/kyr wurden rekonstruiert.

Schlüsselwörter: Paleozän/Eozän Grenze, Nördliche Kalkalpen, Turbidite, kalkiges Nannoplankton, Foraminiferen

Introduction

The base of the prominent (2–3 ‰) negative carbon isotope excursion (CIE) in the upper part of calcareous nannoplankton zone NP9 has been proposed by the International Subcommission of Paleogene Stratigraphy (Luterbacher et al. 2000) to recognize the Paleocene/Eocene-boundary (P/E-boundary). The CIE, which took place at 55.5 Ma and lasted c. 170 kyr (Röhl et al. 2000), has been related to a massive methane release (Dickens et al. 1995, 1997), as a result of the dissociation of submarine methane hydrates (see Dickens 2004, for a review), or thermogenic methane (Svensen et al. 2004) and terrestrial organic carbon (Kurtz et al. 2003), or a combination of these sources (Panchuk et al. 2008; Sluijs et al. 2007a, b). A comet impact was suggested by Kent et al. (2003), however, this theory is largely discarded (Kopp et al. 2007; Lippert & Zachos 2007). The CIE is associated with a global extinction event which affects both marine and terrestrial biota (Sluijs et al. 2007a), most prominently deep–sea benthic foraminifera (see Thomas 1998 and 2007 for reviews), a rapid diversification of planktic foraminifera (Lu & Keller 1993; Kelly et al., 1996, 1998), a global bloom of the dinoflagellate genus *Apectodinium* (Crouch et al. 2001; Sluijs & Brinkhuis 2009; Sluijs et al. 2006), a turnover in calcareous nannoplankton (Bybell & Self-Trail 1994; Gibbs et al. 2006; Raffi et al. 2009), a major turnover in land mammals (Wing et al. 1991; Bowen et al. 2002; Gingerich 2006), and a shoaling of the calcite compensation depth (Dickens et al. 1995; Zachos et al. 2005).

Deposits within the northwestern Tethyan paleogeographic realm, which later formed parts of the Eastern Alps, show significant facies differences during this time period. On the bordering shelves lower Eocene deposits rest with an erosional unconformity on Upper Cretaceous to Paleocene strata. The onset of the regression that caused the stratigraphic gap across the P/E-boundary took place probably in the latest Paleocene (Egger et al. 2009a). In the adjacent Rhenodanubian Flysch basin, at the abyssal Anthering section (N of Salzburg, Fig. 1B), the CIE is associated with the *Apectodinium* acme and the occurrence of *A. augustum* (Egger et al. 2000; Crouch et al. 2001). The CIE-interval is characterized by an increase in siliciclastic hemipelagite sedimentation rate by a factor of 6 and a significant decrease in the frequency and magnitude of turbidity currents entering the basin. Probably, this increase in terrestrially derived input into the basin was a result

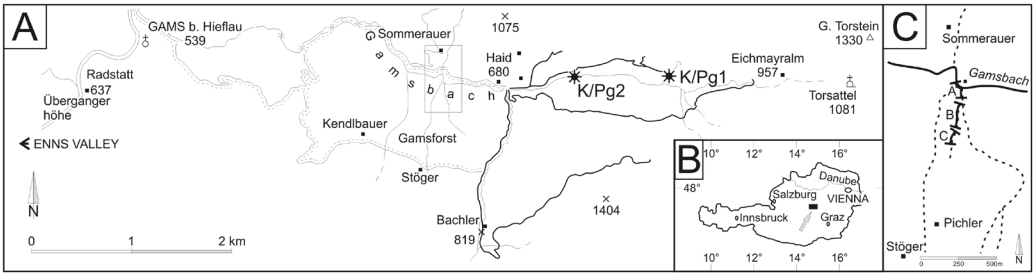

Fig. 1. **A**: Sketch map of the Gams area indicating the investigated section in a southern unnamed tributary creek of the Gamsbach. K/Pg 1 and K/Pg2 mark the Cretaceous/Paleogene boundary sites described by STRADNER & RÖGL (1988), GRACHEV et al. (2005) and EGGER et al. (2009a, b). **B**: Inset map of Austria and location of Gams and Salzburg sections mentioned in the text. **C:** Sketch map indicating detailed location of the investigated sections A, B, and C.

of the low sea-level and associated enhanced continental erosion (EGGER et al. 2003). Increased sediment supply to marine basins was a widespread phenomenon during the PETM (Paleocene Eocene Thermal Maximum) and is interpreted as a response to PETM climate change and critical for carbon and nutrient cycles (see SLUIJS et al. 2008).

At the bathyal Untersberg section (Northern Calcareous Alps SW Salzburg, Fig. 1B), in the dominant marlstone, a 5.5 m thick intercalation of red, green and grey claystone and marly claystone represents the CIE-interval (EGGER et al. 2005). This indicates a substantial shallowing of the calcite compensation depth at that stratigraphic level. An increase in detrital quartz and feldspar within the CIE-interval suggests increased continental run−off from the north.

In this paper, the sedimentary, paleontological and geochemical record of the Pichler section in the Gosau basin of Gams, Styria (see Figs 1A, B; EGGER et al. 2009b) is presented, which provides the longest record across the boundary known from the northwestern Tethyan realm so far. This paper describes in the Paleocene/Eocene boundary interval and the sedimentology and biostratigraphy of this section based on nannofossils, foraminifera and additional dinoflagellate and stable isotope data.

Geological Setting

The Gosau Group of Gams comprises a succession of Upper Cretaceous to Paleogene sedimentary deposits within the Northern Calcareous Alps. In the upper part of the succession, both the Cretaceous/Paleogene (STRADNER & RÖGL 1988) and the Paleocene/Eocene boundary were identified in deep-water deposits (EGGER et al. 2009a; WAGREICH et al. 2009). Recent investigations indicate the presence of a continuous sedimentary record across the Paleocene/Eocene-boundary section within the Zwieselalm Formation (EGGER & WAGREICH, in WAGREICH 2009).

Paleogeographically, the Gosau Group was deposited in the northwestern Tethys realm at a paleolatitude of 20° to 30° N (Wagreich & Faupl 1994). The Gosau Group comprises mainly siliciclastic and mixed siliciclastic-carbonate strata deposited after Early Cretaceous thrusting in the Northern Calcareous Alps. Deposition of the Gosau Group was the result of transtension, followed by rapid subsidence into deep-water environments due to subduction and tectonic erosion at the front of the Austro-Alpine microplate (Wagreich 1993, 2001).

The Gosau basin of Gams is situated in northern Styria, east of the Enns valley (Fig. 1). The main part of the E-W-elongated outcrop belt of Upper Cretaceous to Paleogene strata lies unconformably upon Permian-Triassic to Lower Cretaceous rocks of the Unterberg Nappe (Wagreich et al. 2009).

The Gosau Group of Gams can be divided into two parts – a lower part comprising terrestrial and shallow-water sediments (Lower Gosau Subgroup), and an upper part, comprising deep-water strata (Upper Gosau Subgroup), mainly concentrated in the eastern part of the basin (Kollmann 1964; Wagreich et al. 2009).

The Lower Gosau Subgroup comprises several formations of Late Turonian to Campanian age, and is characterized by abundant macrofossils, including rudist biostromes, coal seams and several key stratigraphic horizons rich in ammonites and inoceramids (Summesberger & Kennedy 1996; Summesberger et al. 1999; Wagreich 2004). The overlying deep-water sediments of the Upper Gosau Subgroup are assigned to the Nierental Formation (Campanian-Danian; Wagreich & Krenmayr 1993; Summesberger et al. 2009) and the Zwieselalm Formation (Danian-Ypresian; Egger et al. 2004). The biostratigraphy was mainly based on planktic foraminifera, which provide evidence for a range well into the Paleogene as recognized for the first time by Wicher (1956). Later, Kollmann (1963, 1964) gave a detailed foraminiferal zonation and recognized a nearly continuous section from the Campanian up to the lower Eocene. Several Cretaceous/Paleogene (K/Pg) boundary sites in the eastern Gams basin have been investigated in detail, i.e. Stradner & Rögl (1988), Lahodynsky (1988a, b), Grachev et al. (2005, 2008), Grachev (2009), Wagreich (2009) and Egger et al. (2009a, b).

The Paleogene succession (Fig. 2) ranges up to the lower Eocene (NP12; Egger & Wagreich 2001) and is punctuated by stratigraphic gaps, which comprise zone NP3 and parts of zones NP6 to NP8 in some of the sections (Egger et al. 2004). The K/Pg-boundary interval and the Danian deposits of the Nierental Formation are characterized by the predominance of red and grey pelagic to hemipelagic marlstones and marly limestones with thin turbidites and single debris flows (Egger et al. 2004, 2009a). This interval is followed by a turbidite-dominated unit assigned to the Zwieselalm Formation (Wagreich et al. 2009). Within this formation, a continuous Paleocene/Eocene boundary section is exposed in a creek in the eastern part of the Gams basin (Egger & Wagreich, in Wagreich 2009). The creek forms a southern tributary of the Gamsbach (Krautgraben) to the west of Haid, south of farm house Sommerauer (Figs 1A, C; UTM coordinates: 014° 50’ 25’’ E, 47° 39’ 40’’ N). The so-called Pichler section (named after the farm house Pichler south

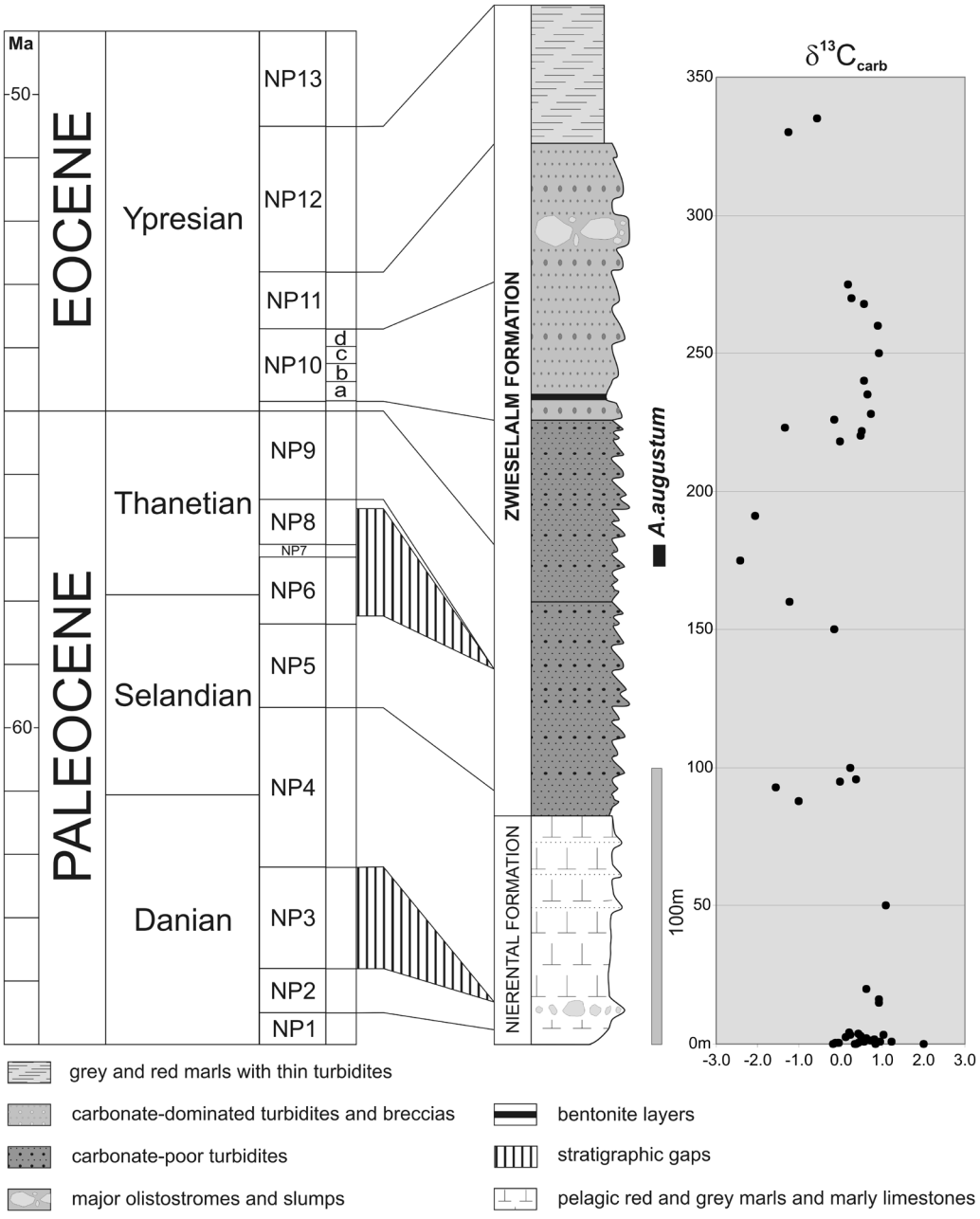

Fig. 2. General stratigraphic log of the Paleogene of Gams, including carbon isotope data of carbonates and the range of *Apectodinium augustum*. Modified from WAGREICH (2009).

Table 1. Counts and estimates of planktic and benthic foraminifera. Estimates: r = rare, 1-5 %; f = frequent, 5-20 %; a = abundant, >20 %.

			Planktic foraminifera									Benthic foraminifera								
Sample	net weight (gr)	Split	*Acarinina* spp.	*Chiloguembelina* spp.	*Globanomalina* spp.	*Morozovella* spp.	*Parasubbotina* spp.	*Planorotalites* spp.	Subbotina *spp.*	Sum planktic	lensiform	biserial	elongated	triserial	agglutinated species	Sum benthic	% planktic species	no. of foram. picked	ind/gr
PEG-01	200	1	16	2	6		5	8		37	31	3	3		1	38	49	75	0.38
PEG-02	200	64	7			2	31		19	59	8					8	88	67	21.44
PEG-03	200	512	66	37	3	54	120	163	10	453	41	3		20		64	88	517	1323.52
PEG-04	200	128	104	41	13	46	130	69	28	431	93	21	1	35	2	152	74	583	373.12
PEG-05	200	512	47	13	7	46	14	31	6	164	52	14	4	10		80	67	244	624.64
PEG-06	200	32	a	f		r	a	a			a	r	r	r				916	146.56
PEG-07	200	32	f			r		f			a		r					92	14.72
PEG-08	200	16	f	f		r	a	a			a	f	r	f				794	63.52
PEG-09	200	64	a	f		r	a	a			a	f	r	f				915	292.80
PEG-10	200	128	a	r		r	r		r		a							157	100.48
PEG-11	200	256	a	f		r	a	a			f	r	r	f				374	478.72
PEG-12	200	2	f	r			f	f				r			f			98	0.98
PEG-13	200	512																0	0.00
PEG-14	200	16																14	1.12
PEG-15	200	32	a	f			a	a			f	r		r				318	50.88
PEG-16	200	2048																4	40.96
PEG-17	200	32	a	a			a	a			a	r	f	f	r			513	82.08
PEG-18	200	1024																1	5.12
PEG-19	200	128																19	12.16
PEG-20	200	32																4	0.64
PEG-21	200	32	r	r		r	f				f	r			r			51	8.16
PEG-22	200	64																5	1.60
PEG-23	200	128																2	1.28
PEG-24	200	64																4	1.28
PEG-25	200	64																4	1.28
PEG-26	200	256																6	7.68
PEG-27	200	256																1	1.28
PEG-28	200	256																0	0.00
PEG-29	200	256	2				2	1	4	9	7	2				9	50	18	23.04
PEG-30	200	32																0	0.00
PEG-31	200	64																0	0.00
PEG-32	200	4																0	0.00
PEG-33	200	32																0	0.00
PEG-34	200	256									1				1			2	2.56
PEG-35	200	32	a	a			a	a			a							369	59.04
PEG-36	200	1								0					319	319	0	319	1.60
PEG-37	200	128		r			f	r			f				r			58	37.12
PEG-38	200	64	3			2	5			10	8	1	1		9	10	50	29	9.28

of the creek) starts at the confluence of the Gamsbach and the tributary creek including the cut bank of the Gamsbach itself (section A, Fig. 1C; UTM coordinates 014° 50' 26'' E, 47° 39' 49'' N) with a ca. 34 m thick section. Above a few meters covered by debris and vegetation, a continuous, ca. 43 m-thick section starts within the western branch of the creek (section B, Fig. 1C), which includes the Paleocene/Eocene boundary interval. Overlying section B, above a 10 m unexposed interval, section C exposes another 27 m of section. The top (UTM coordinates 014° 50' 27'' E, 47° 39' 35'' N) is overlain by Quaternary moraine.

Materials and Methods

Sampling within the creek was performed during several field campaigns between 2006 and 2009. A total of 120 samples were taken from the section and the neighbouring creek mainly for nannofossil and foraminiferal biostratigraphy. Some of the samples were also used for dinoflagellate biostratigraphy, geochemistry and stable isotope measurements. Samples and slides are stored at the Geological Survey (GBA2011/002/0001).

Calcareous Nannofossils

Smear-slides were prepared from a suspension of unprocessed material in distilled water of pH 7 without applying concentration techniques. The smear slides were studied under a Zeiss Axioplan light microscope using crossed and parallel polarization filters at a magnification of 1000x.

Foraminifera

Two hundred gram of sample material (samples with prefix PEG) were soaked with 5 % hydrogen peroxide for disintegration and washed through a 0.063 mm sieve. Aliquots (splits) were scanned and picked for foraminifera classification. In addition, complete >0.250 mm fractions gained by dry-sieving were scanned for biostratigraphic index species (mainly planktic species) and potential paleoecologic indicators (agglutinated species). Almost all samples show intensively sorted assemblages, pointing to a strong influence of transportation processes. The larger size fractions are missing in almost all samples and only the fraction slightly above 0.063 mm is present in most samples. As a result of the transportation processes, specimens are frequently worn out or, due to their small size, difficult to identify. Consequently, we only estimated the percentages of genera (planktic foraminifera) or morphologic groups (benthic foraminifera) of many samples. All counts and estimates are listed in Tables 1 and 2. Autochthonous assemblages are assumed for only those two samples, which contain also the large size fractions: PEG-05 at section meter 110.96, and PEG-36 at section meter 10.30.

Table 2. Foraminiferal species distribution in autochthonous samples PEG-05 and PEG-36. In sample PEG-36, 39 fragments have been counted for *Arthrodentron diffusum*. They may represent only one specimen.

PEG-05		
Species	ind.	%
Acarinina cf. *esnaensis* (LeRoy, 1953)	1	1
Acarinina soldadoensis (Brönnimann, 1952)	33	20
Acarinina subshaerica (Subbotina, 1947)	13	8
Chiloguembelina crinita (Glaessner, 1937)	2	1
Chiloguembelina trinitatensis (Cushman & Renz, 1942)	11	7
Globanomalina cf. *chapmani* (Parr, 1938)	7	4
Morozovella acuta (Toulmin, 1941)	3	2
Morozovella aequa (Cushman & Renz, 1942)	20	12
Morozovella apanthesma (Loeblich & Tappan, 1957)	1	1
Morozovella occlusa (Loeblich & Tappan, 1957)	2	1
Morozovella subbotinae Morozova, 1939	20	12
Parasubbotina varianta (Subbotina, 1953)	14	9
Planorotalites pseudoscitula (Glaessner, 1937)	31	19
Subbotina triangularis (White, 1928)	6	4
Sum planktic foraminifera	164	100
Aragonia velascoensis (Cushman, 1925)	2	3
Bolivina cf. *midwayensis* Cushman, 1936	12	15
Bulimina cf. *bradbury* Martin, 1943	5	6
Bulimina cf. *trinitatensis* Cushman & Jarvis, 1928	5	6
Cibicidoides cf. *tuxpamensis* (Cole, 1928)	30	38
Gavelinella cf. *farafraensis* (LeRoy, 1953)	3	4
Gavelinella cf. *micra* (Bermudez, 1949)	2	3
?*Gavelinella* sp.	4	5
Gavelinella danica (Brotzen, 1940)	6	8
Gyroidinoides cf. *girardenus* (Reuss, 1851)	2	3
Hanzawaia cushmani (Nuttall, 1930)	2	3
Planularia sp.	3	4
Stilostomella gracillima (Cushman, 1933)	2	3
Stilostomella subspinosa (Cushman, 1943)	2	3
Sum benthic foraminifera	80	100

PEG-36		
Species	ind.	%
Ammodiscus glabratus Cushman & Jarvis, 1928	5	2
Ammodiscus siliceus (Terquem, 1862)	6	2
Arthrodendron diffusum (Ulrich, 1904)	39	12
Dolgenia sp.	1	0
"Glomospira" irregularis (Grzybowski, 1898)	20	6
Glomospirella gaultina (Berthelin, 1880)	3	1
Hormosina velascoensis (Cushman, 1926)	7	2
Hyperammina cf. *nuda* Subbotina, 1950	3	1
Kalamopsis grzybowskii (Dylasanka, 1923)	1	0
?Nothia sp.	10	3
Placentammina placenta (Grzybowski, 1898)	12	4
Psammosiphonella cylindrica (Glaessner, 1937)	28	9
Psammosphaera fusca Schulze, 1875	3	1
Recurvoides sp.	36	11
Reophax cf. *minuta* Tappan, 1940	1	0
Reophax duplex Grzybowski, 1896	2	1
Reophax subnodulosus Grzybowski, 1898	15	5
Subreophax sp.	12	4
Thalmannammina subturbinata (Grzybowski, 1898)	35	11
Trochammina sp.	12	4
Trochamminoides dubius (Grzybowski, 1901)	7	2
Trochamminoides proteus (Karrer, 1866)	46	14
Trochamminoides variolarius (Grzybowski, 1898)	15	5
Sum	319	100

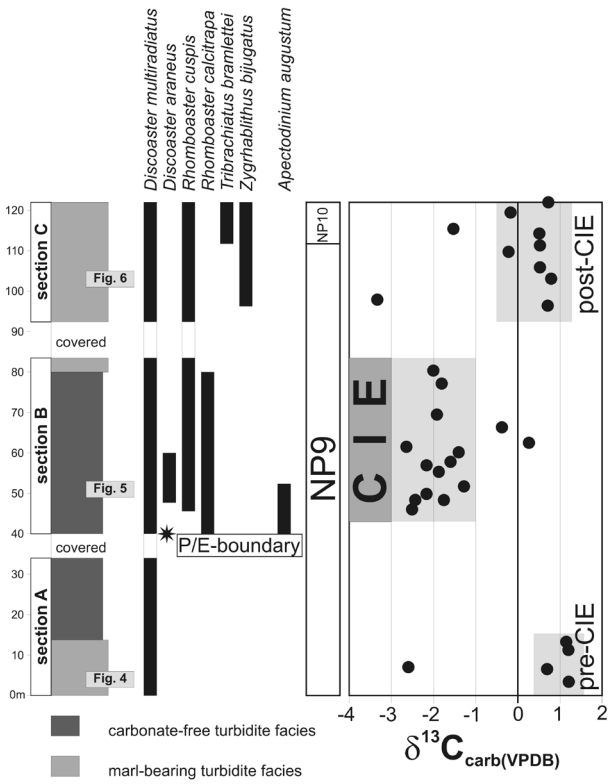

Fig. 3. Detailed composite overview log of the studied section with sections A, B and C marked, main biostratigraphic markers (nannofossils, dinoflagellates) recognized, and carbon isotope data of bulk carbonate. Positions of detailed sections of figs. 4 to 6 indicated in log.

Dinoflagellates

For dinoflagellate studies, thirty grams of each sample were processed following standard procedures (e.g. WOOD et al. 1996). 20 gram of dry sediment were crushed and treated with cold 35 % HCl for one day, to remove carbonates. Decantation was carried out two times, with added water with a minimum interval of six hours. These samples were also treated with 38 % HF for one day to remove silicates. Two decantations with a minimum interval of seven hours followed, with added water each time and a minor amount of 35 % HCl, to the samples to remove the gel that may have formed during the previous step. Water was added for a final time after which the sample were placed in an ultrasound tank for 30 s. Subsequently, the samples were sieved over a 15 µm mesh nylon sieve. A part of residue was mounted in glycerine jelly on 4 microscope slides (a, b, c, d) after extensive mixing to obtain homogeneity and covered with slide cover (20 x 40 mm).

Geochemistry

Carbonate and organic carbon contents were measured using a LECO carbon analyzer and a gas-volumetric method. The chemical composition (Tab. 3) of concretion samples (whole-rock major and minor elements) was analyzed at the geochemical laboratory of the Geological Survey of Austria.

The stable isotopic composition of bulk carbonate samples was analyzed on 0.1–0.3 mg untreated samples using the phosphoric acid reaction. Samples were prepared on-line using a Gasbench II interfaced to a ThermoFisher CF-IRMS. Calibration of the mass spectrometer was performed against VPDB using an in-house marble standard calibrated against the international reference standard NBS 19 and results are reported in the delta notation. The analytical error (1 s.d.) for $\delta^{13}C$ and $\delta^{18}O$ based on the long-term performance of quality assurance material is 0.06 and 0.08‰, respectively (see Spötl & Vennemann 2003).

Sedimentology and Geochemistry

Description of the Section

The Pichler section is dominated by sandy to silty turbidites. Significant differences in rock composition result from variations in carbonate content and the presence and absence of conspicuous marl layers. Based on these features, a lower carbonate-bearing and coarser grained interval can be recognized, followed by a carbonate-poor, finer-grained interval around the Paleocene/Eocene boundary that again grades into a more carbonate-rich interval at the top of the section (Fig. 3). Transitions from one interval to the other occur over several meters to tens of meters. Therefore, no exact positions of boundaries between those facies types can be given within the section.

The lowermost ca. 13 m of the section (section A, outcrop at cut bank of Gamsbach) are characterized by several up to 110 cm-thick sandy turbidites with clear grading from a gravel-dominated base (components up to 7 cm) to a fine sandstone/siltstone top. Bouma intervals T_a to T_e are present, sometimes with prominent convolute lamination (Fig. 4). The sandy parts of the turbidite beds grade within a few centimeters into dark grey silty claystones. Thin turbidite sandstone to coarse siltstone beds (0.5 to 30 cm) are present between these thick beds which constitute the majority of the turbidites present. Thicker beds display complete Bouma sequences whereas thin beds mostly show the Bouma interval T_{cde}. Amalgamation of several turbidite beds to single thick beds is a common feature. Some clasts of Paleocene platform limestones are present in the turbidite layers (Fig. 4c).

A 15 cm-thick mud-supported debris flow bed with a silty-clayey matrix and clasts up to 5 cm in diameter is present. Another conspicuous feature of this basal part are up to 80 cm-thick marl beds (mean carbonate content of five samples 12.4 wt%, maximum

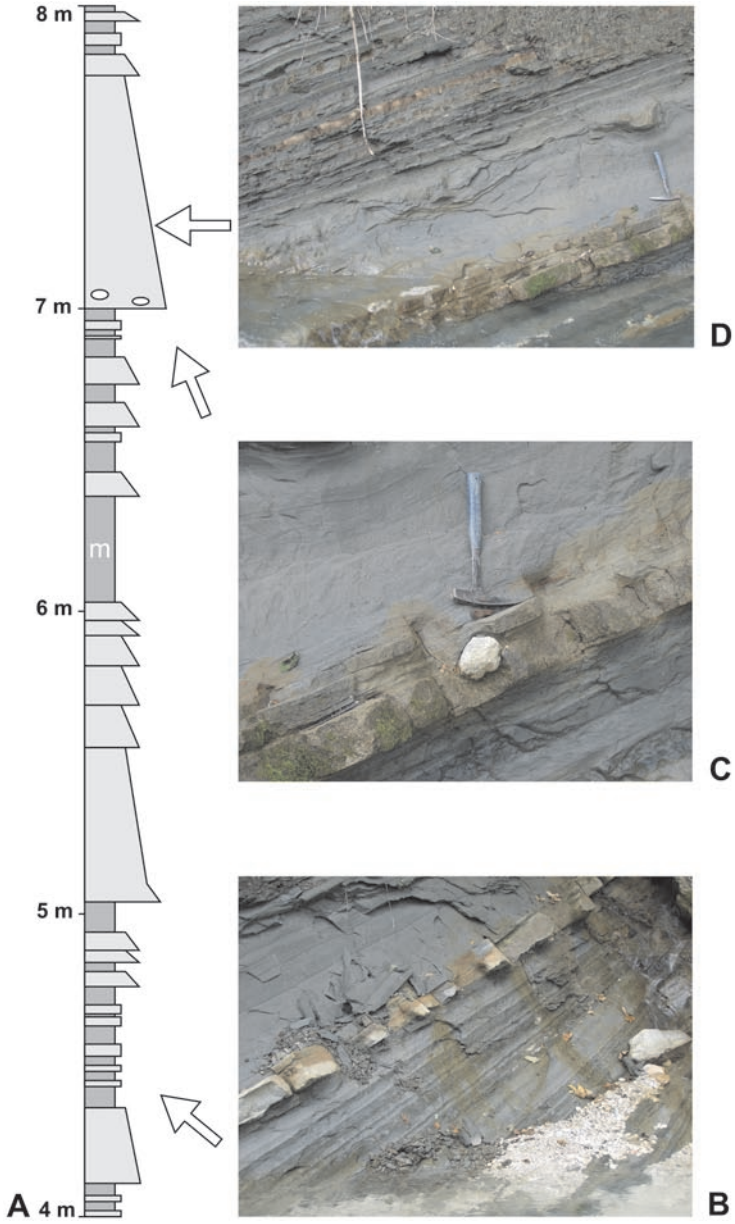

Fig. 4. **A**: Detailed sedimentological log from the lower part of section A (4.00 to 8.00 m; white m denotes marl beds). **B–D**: Photographs of typical facies types from this section (arrows point to position of photographs within the section).

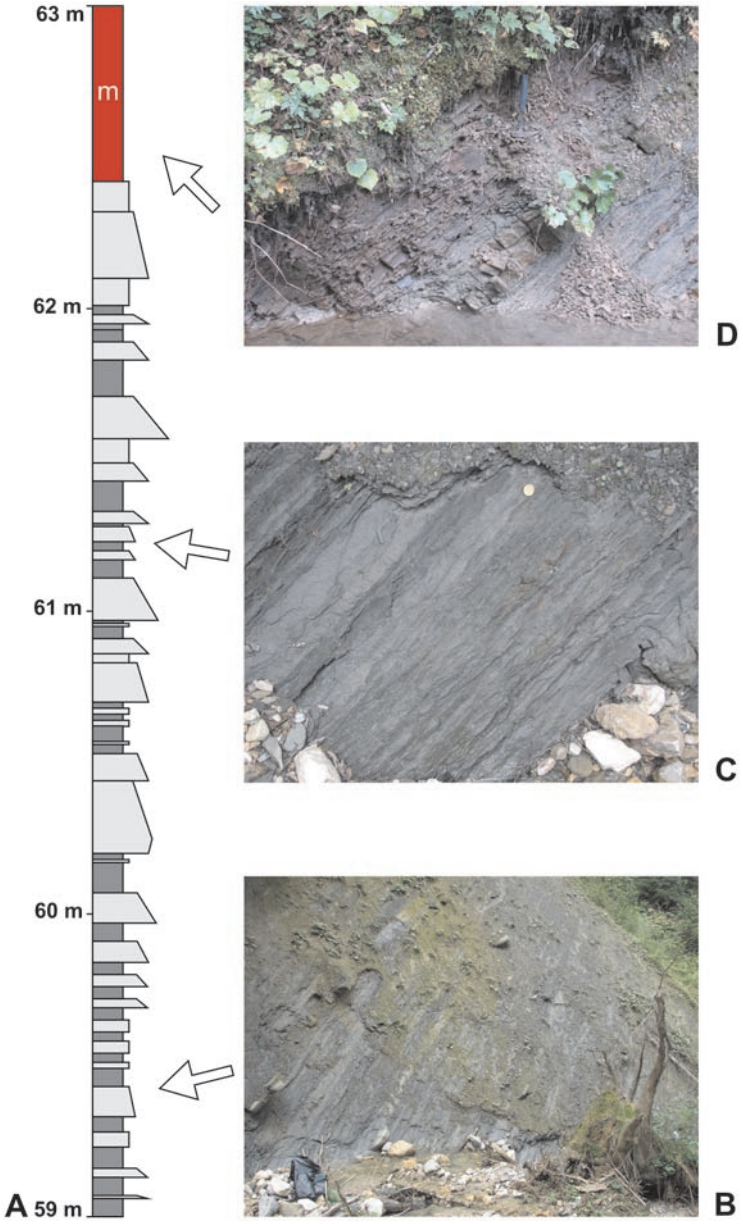

Fig. 5. **A**: Detailed sedimentological log from the middle part of section B (59.00 to 63.00 m; white m denotes reddish marl bed). **B–D**: Photographs of typical facies types from this section (arrows point to position of photographs within the section).

16.7 wt%) without any visible bedding. The top parts of these marl beds as well as some of the dark grey thin silt-clay layers show downward bioturbation by mainly *Chondrites*-type burrows.

Sandstone/pelite ratios are between 1:1 to 2:1. The turbidites, especially the thin sandy layers, display only weak cementation due to a low carbonate content. Turbiditic shales are dark grey, mainly only a few centimeters thin, and largely devoid of carbonate. No clear fining- or coarsening-upward cycles could be recognized; only at meter 5 of the section a 1 m-thick succession of six amalgamated turbidite beds display a fining-upward and thinning-upward trend.

The turbidite facies is characterized by classical sandy turbidites showing both complete and incomplete, base-truncated Bouma sequences. This corresponds to facies C and D of WALKER (1978) and, according to the classification of PICKERING et al. (1989), these sandstones fall into the classical turbidite facies C2 (organized sand-mud couplets – classic turbidites). The thick sandstone beds show characteristics for transitional deposition from relatively low- to high-concentrated and high-density turbidity currents. The dark grey clays are interpreted as representing the fine-grained portion of the turbidites. The thicker marl beds present may be interpreted either as (fine-grained) turbidites or hemipelagites. Several observations argue for an origin as a turbidity current: (1) these marl beds follow directly above turbiditic sandstone beds, (2) at 2.5 m in the section 15 cm-thick pebbly mudstone directly grades into a 80 cm-thick marl bed; (3) foraminiferal data (see below) also support a transported microfauna and thus argue against a hemipelagic deposition of these marl beds.

This marl-bearing interval grades in the top part of section A into an interval without distinctive marl beds, which ranges up to the upper part of section B, up to ca. section meter 80. There, thin-bedded sandy- to silty turbidites with thin, dark-grey silty claystone intervals prevail (Fig. 5B). Claystones to marly claystones have carbonate contents of 0 to 6.4 wt% (mean of 28 samples 1.9 wt%). A few sandstone beds up to 48 cm are present but the majority of sandstone layers are only a few centimeters thin. Grading is ubiquitous and thicker sandstones show complete T_{a-e} Bouma sequences; thinner beds often show only T_{cd} intervals. Two distinctive reddish brown marly claystone to marl beds (22.9 and 34.2 wt% carbonate content) of up to 85 cm thickness are present at 62 and 66 m of the section. Bioturbation has only very rarely been observed.

Sandstone/pelite ratios are between 2:1 to 5:1.This facies is interpreted as mainly thin-bedded classical turbidites in the sense of WALKER (1978: facies D) and PICKERING et al. (1989; facies C2.2 and C2.3). The lack of identifiable hemipelagic layers and the high proportion of sand suggests a high-frequency turbidite environment. The reddish claystone layers probably also represent turbidites, i.e. mud turbidites, as also suggested by a transported and poor microfauna (see below).

Starting at around 80 m in the section, light grey to slightly greenish grey marly claystones and marl beds again occur and become significant, and sandstone beds become thicker

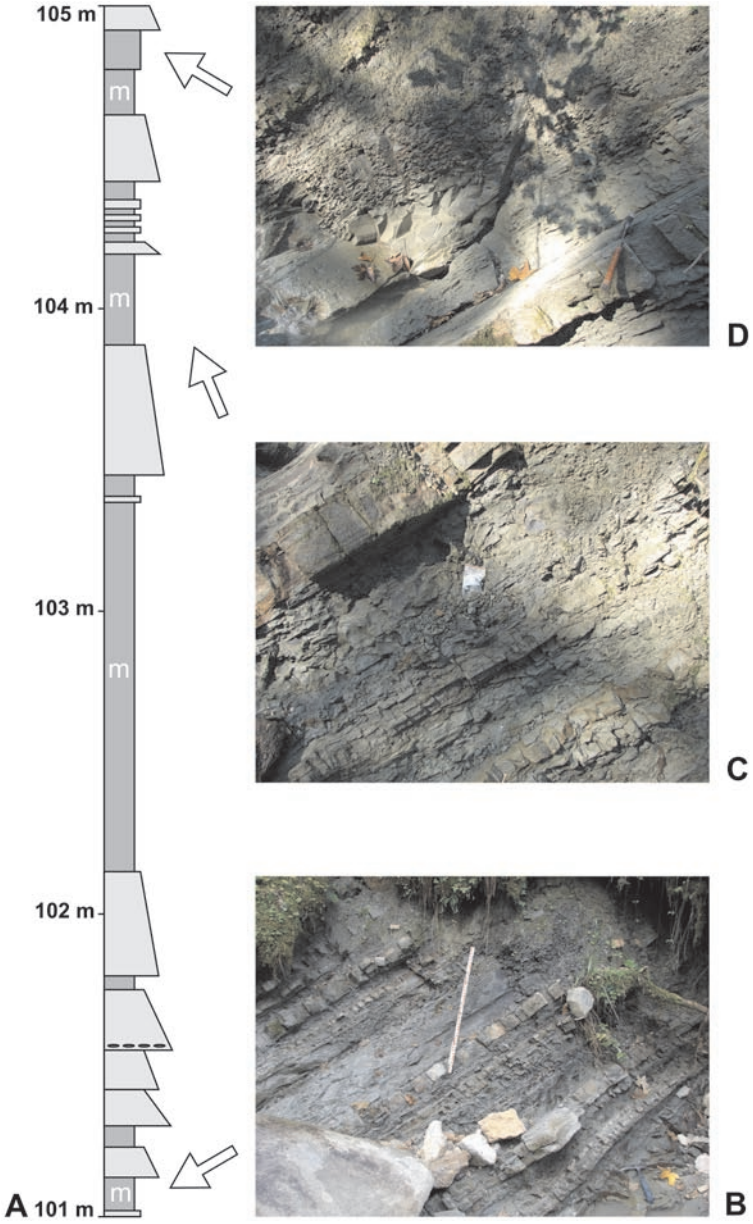

Fig. 6. **A**: Detailed sedimentological log from the middle part of section C (101.00 to 105.00 m; white m denotes marl bed). **B–D**: Photographs of typical facies types from this section (arrows point to position of photographs within the section; scale in lower right 90 cm).

Table 3. Chemical composition (wt%) of siderite concretions, concretional layers and surrounding fine-grained sediments.

	rusty Fe-crust	rusty layer	hard concretion layer	lowermost concretion	concretion
Bezeichnung	GAMS-17-09	GAMS-18-09	GAMS-19-09	GAMS-20-09	GAMS-24b-09
SiO_2 (%)	37.3	21.0	27.7	37.7	10.1
TiO_2 (%)	0.665	0.40	0.47	0.673	0.1
Al_2O_3 (%)	9.6	8.14	9.91	12.2	3.5
FeO (%)	8.27	33.86	28.67	21.86	41.1
$FeCO_3$ (%)	13.35	54.62	46.25	35.26	66.36
MnO (%)	0.57	0.42	0.94	0.55	2.12
MgO (%)	2.0	2.8	2.6	2.5	2.9
CaO (%)	19.9	4.8	5.0	3.8	6.0
Na_2O (%)	0.9	< 0.5	< 0.5	0.8	< 0.5
K_2O (%)	1.49	1.18	1.54	2.07	0.5
$H_2O^{110° C}$ (%)	0.6	0.7	1.1	1.35	0.4
H_2O+ (%)	0.7	< 0.1	< 0.1	0.98	< 0.1
P_2O_5 (%)	0.87	1.85	2.27	1.65	2.07
CO_2 (%)	16.3	24.9	20.1	13.7	31.7
SO_3 (%)	0.04	0.06	0.13	0.13	0.08
sum	99.3	100.1	100.5	100.1	100.6
As (ppm)	2	5	3	4	3
Ba (ppm)	254	277	271	964	113
Cd (ppm)	< 1	<1	< 1	< 1	< 1
Co (ppm)	< 5	< 5	< 5	< 5	< 10
Cr (ppm)	72	26	25	51	< 5
Cs (ppm)	< 1.5	< 1.5	< 1.5	< 1.5	< 1.5
Cu (ppm)	14	18	23	25	14
Nb (ppm)	14	9	9	13	4
Ni (ppm)	22	20	29	39	11
Pb (ppm)	8	< 7	7	10	< 10
Rb (ppm)	56	56	74	95	25
Sr (ppm)	314	361	215	208	180
V (ppm)	63	104	93	121	26
Y (ppm)	30	78	85	98	49
Zn (ppm)	48	61	63	81	43
Zr (ppm)	136	73	80	131	29
sum (ppm)	1032	1087	976	1842	497

again (up to 80 cm). This facies resembles largely the basal interval; however, the carbonate contents rises significantly: the mean of nine samples of marl layers above 90 m in the section is 19.7 wt% and the maximum is 29.0 wt%. Although cm-thick sandstone turbidite beds are still present, thicker sandstones and marls predominate the topmost part of the section above 100 m (Fig. 6). Convolute bedding and structures indicative of water-escape processes such as flame and ball-and-pillow structures are often present in the sandstones. Amalgamation of beds is commonly observed. Flute casts indicate a

Table 3. (continued)

	5 cm concretion	concretion	6 cm claystone	7 cm hemipelagic claystone
Bezeichnung	GAMS-26-09	GAMS-07-09	GAMS-24a-09	GAMS-25-09
SiO_2 (%)	33.4	11.8	57.5	60.0
TiO_2 (%)	0.612	0.151	1.1	1.2
Al_2O_3 (%)	10.6	3.8	18.3	18.5
FeO (%)	26.0	37.04	7.6	6.3
$FeCO_3$ (%)	41.88	59.75	12.19	10.16
MnO (%)	1.2	1.16	0.04	0.04
MgO (%)	2.7	3.4	2.8	2.8
CaO (%)	2.5	9.8	0.9	0.8
Na_2O (%)	0.7	< 0.5	1.3	1.3
K_2O (%)	1.64	0.5	3.4	3.1
$H_2O^{110° C}$ (%)	0.9	0.7	2.2	1.7
H_2O+ (%)	< 0.1	< 0.1	4.3	3.6
P_2O_5 (%)	0.16	1.17	0.13	0.1
CO_2 (%)	18.5	30.6	1.1	1.0
SO_3 (%)	0.037	0.10	0.11	0.29
sum	98.9	100.2	100.6	100.6
As (ppm)	3	5	4	7
Ba (ppm)	273	287	527	510
Cd (ppm)	< 1	< 1	< 1	< 1
Co (ppm)	< 10	< 5	10	11
Cr (ppm)	34	< 5	135	141
Cs (ppm)	< 1.5	< 1.5	4	< 1.5
Cu (ppm)	20	15	32	27
Nb (ppm)	13	3	23	23
Ni (ppm)	28	18	63	76
Pb (ppm)	7	< 8	23	24
Rb (ppm)	73	28	155	142
Sr (ppm)	79	171	98	95
V (ppm)	84	23	197	192
Y (ppm)	19	41	27	26
Zn (ppm)	67	40	112	108
Zr (ppm)	118	29	218	230
sum (ppm)	818	659	1627	1613

paleotransport direction from SW to NE. Marl beds up to 120 cm thick are intercalated. Foraminiferal data indicate that at least some of the marl beds represent hemipelagites as suggested by an autochthonous foraminiferal assemblage with abundant planktic foraminifera (see below).

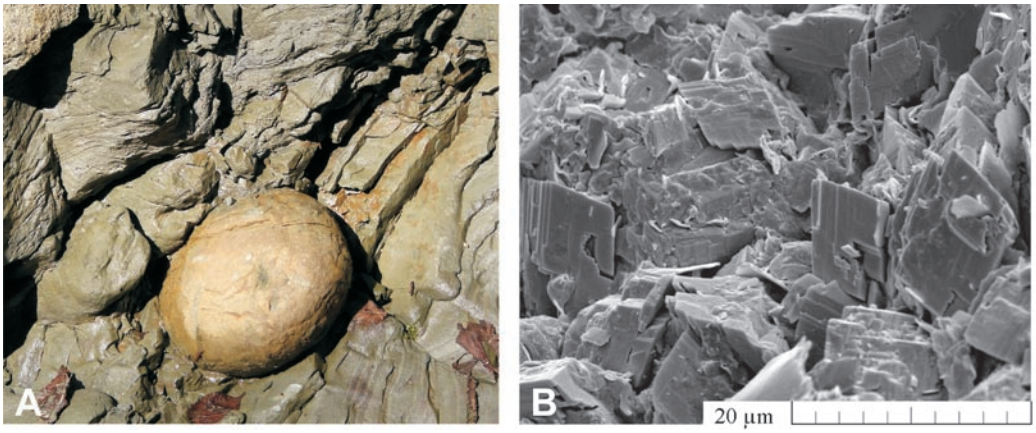

Fig. 7. **A**: Siderite concretion (13 cm in diameter), outcrop in middle part of section B, within largely carbonate-free turbidites. **B**: REM picture of diagenetic siderite from concretion in section B.

Results

Sedimentation below the local calcite compensation depth (CCD) is very probable for the lower part of the section (up to ca. 70 m) given the overall very low amount of carbonate in the turbidites and the lack of distinctive marly hemipelagites. Even mud turbidites within the middle interval are largely devoid of carbonate. Due to a shallowing of the depositional area and/or a deepening of the CCD the upper part of the section (upward from ca. 80 m) was deposited above the CCD. This is in accordance with the general trend in the Paleogene of Gams which shows a transition into an interval dominated by carbonate turbidites further-up section (EGGER et al. 2004).

Siderite concretions

A prominent feature of the Paleocene/Eocene-boundary interval are siderite concretions, which are conspicuous in outcrops due to their hardness and rusty color (Fig. 7). Concretions occur within several levels both in sandy-silty and in silty-clayey material, especially in the middle part of the section. Both, layers enriched in disseminated siderite cement and platy to rounded ellipsoid siderite nodules up to 30 cm in diameter are present.

Table 3 shows the geochemistry of concretion samples and surrounding fine-grained sediments. Siderite ranges up to a maximum of 66 wt% within the concretions (41.1 wt% FeO). Mudstones embedding the concretions show FeO values around 6 – 8 wt%. No significant enrichment in minor elements was observed. A pre-compaction origin of the concretions is evident by the presence of squeezed sedimentary layering around the nodules. Although detailed investigations are missing, an early diagenetic origin of the siderite is probable (e.g. LAENEN & DE CRAEN 2004).

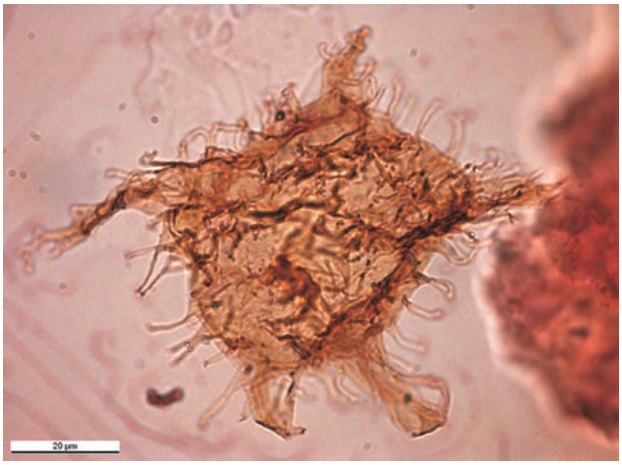

Fig. 8. *Apectodinium augustum* (Harland, 1979) Lentin & Williams, 1981, a dinoflagellate typical for the Paleocene/Eocene-boundary interval; Pichler section, 40 m. Scale bar = 20 µm.

Carbon isotope stratigraphy

Stable isotope measurements of whole-rock samples (Figs 2, 3) are influenced by diagenesis and the small amount of carbonate of the samples, which can be as low as 0.1 %. The oxygen isotope values range between -1.0 and -5.5 ‰ and are considered to be strongly influenced by diagenesis as no systematic variation could be recognized within the section. Carbon isotope values range from +1.2 to -8.9 ‰. This large variation is considered to be also influenced by diagenesis and the low carbonate content and highly negative values below -8 ‰ are not considered further. However, except for a few outliers, a clear trend can be seen in the section. The lower part (up to 15 m) is characterized by values around 0.5 ‰ (mean of six samples 0.43 ‰). A gap with virtually no carbonate occurs up to ca. 45 m. The following ca. 40 m-thick interval is characterized by slightly negative values around -2 ‰ (mean of 15 samples -1.7 ‰). After another gap due to a covered section interval, above 90 m, values increase again to ca. 0.5 ‰ (mean of 10 samples -0.14 ‰).

Based on these data and the extended stratigraphic range of marker species we speculate that the CIE of the PETM (e.g. Zachos et al. 2007) is represented by a strongly expanded section of at least 35 m and present between 45.7 and 80 m. As no isotope data are available from the 33 m-thick interval below 45.7 m due to the lack of carbonate and a covered section interval, the CIE may well comprise an interval thicker than 35 m.

Biostratigraphy

The biostratigraphic evaluation of the Pichler section is handicapped by the presence of two unexposed intervals, the paucity of carbonate especially in the middle part of the section, and the predominance of turbidites, which result in mostly allochthonous microfossil assemblages. Therefore, both calcareous nannofossil biostratigraphy and especially

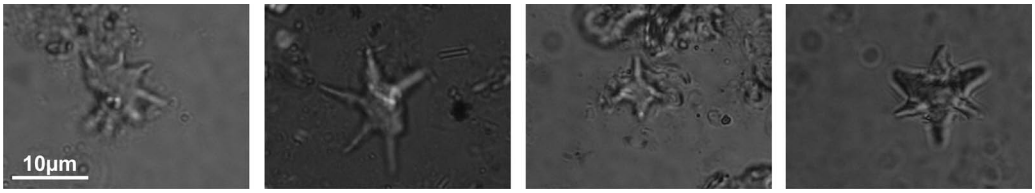

Fig. 9. Nannofossil marker species from the Pichler section (light microscope, magnification 1000x, all same scale): **A**: *Discoaster araneus* BUKRY, 1971 (sample PE4–07, 57.62 m); **B**: *Rhomboaster calcitrapa* GARTNER, 1971 (sample PE7–07, 51.66 m); **C**: *Rhomboaster cuspis* BRAMLETTE & SULLIVAN, 1961 (sample PE14–08, 109.50 m); **D**: *Tribrachiatus bramlettei* (BRÖNNIMANN & STRADNER, 1960) PROTO DECIMA et al. 1975 (sample PE18–08, 115,14 m).

planktic foraminiferal zonations had to be applied with caution. In addition, some of the samples, especially around the suspected P/E-boundary, were also tested for dinoflagellates. The characteristic dinoflagellate *Apectodinium augustum* (Fig. 8) was found in several samples from 40 to 52.50 m (Fig. 3), a clear indicator of the P/E-boundary interval (EGGER et al. 2000; CROUCH et al. 2001; SLUIJS et al. 2006, 2007b, 2008), thus providing additional biostratigraphic information for the nearly carbonate-free interval at the base of section B.

Nannofossils

The distribution of nannofossil marker species (Fig. 9) indicates the presence of the *Discoaster multiradiatus* Zone (Zone NP9) and the *Tribrachiatus contortus* Zone (Zone NP10) in the the Standard Tertiary zonation of MARTINI (1971) (Fig. 3). In the lower part of the section *Discoaster multiradiatus* occurs regularly. Above a 6 m long unexposed interval, the first *Rhomboaster calcitrapa* was found at 40.40 m and the first *Rhomboaster cuspis* at 45.70 m. The first occurrence of the genus *Rhomboaster* is in the upper third of Zone NP9 and coincides with the onset of the CIE-interval (e.g. AUBRY 1996) and, therefore, is a good tool to recognize the P/E-boundary. Another indicator for the CIE-interval is the asymmetrical *Discoaster araneus* whose stratigraphic range is restricted to this interval (e.g. TREMOLADA & BRALOWER 2004). *Discoaster araneus* appears for the first time at 47.76 m and ends at 59.92 m of the section. *Zygrhablithus bijugatus*, a holococcolith species, has its first occurrences in the upper part of Zone NP9 (BOWN 2005) but becomes common not before the P/E-boundary (BRALOWER 2002). At the Pichler section, this species is common from 96.20 m to the top of studied section. The base of NP10 was identified by the first appearance of *Tribrachiatus bramlettei* at 110.90 m.

Foraminifera

Only two samples are considered to represent almost completely autochthonous foraminiferal assemblages. Sample PEG-36 from near the base of the section at 10.3 m contains a number of rather large agglutinated foraminifera (Plate 1). Some of the species provide limited biostratigraphic control in flysch deposits (Geroch & Nowak 1983). *Reophax subnodulosus* points to an Eocene age but the commonly observed early Eocene *Glomospira*-acme (up to 50% according to Kaminski 2005) was not found in the entire section (only 7% in sample PEG-36, even less in other samples). Therefore, a transitional late Paleocene to early Eocene age is assumed for this assemblage.

Sample PEG-05 from the upper portion of the section at c. 110.96 m contains a number of planktic foraminifera that were used for age classification (Plate 2). In particular the concurrent presence of the species *Subbotina velascoensis, Acarinina soldadoensis, Morozovella acuta, M. aequa, M. apanthesma, M. occlusa, M. gracilis* and *M. subbotinae* point to the latest Paleocene – earliest Eocene planktic Zone P5 (Olsson et al. 1999; Pearson et al. 2006) as defined in Berggren et al. (1995). We could not apply the revised zonation of Berggren & Pearson (2005) because index species such as *Acarinina sibaiyaensis* or *Pseudohastigerina wilcoxensis* were not found in the samples. From the foraminiferal point of view, it remains unclear whether this sample is of Paleocene or of Eocene age. The benthic *Aragonia velascoensis* restricts the youngest possible age to zone P5 (Tjalsma & Lohmann 1983).

The combined age of the two autochthonous samples from base and top of the section, both late Paleocene-early Eocene, and the thickness of the strata confirm the high sedimentation rates assumed for this turbiditic depositional environment.

Discussion and conclusions

The occurrences of the dinoflagellate cyst *Apectodinium augustum* and the calcareous nannoplankton species *Discoaster araneus*, *Rhomboaster* spp. and *Tribrachiatus bramlettei* are indicative for the Paleocene-Eocene transition at the Pichler section. Additionally, a negative carbon isotope excursion can be interpreted as the CIE-interval at the base of the Eocene. Using the isotope and paleontological records the thickness of the CIE-interval can be estimated as at least 40 m at the Pichler section

Given a 40 m-thick interval that marks the CIE in the Pichler section and the 170 to 210 kyr duration of that interval (Röhl et al. 2000, 2007; Abdul Aziz et al. 2008; Westerhold et al. 2009; Murphy et al. 2010) a sediment accumulation rate of 19 to 23.5 cm/kyr can be calculated. Even higher accumulation rates are calculated by applying shorter duration estimates as reported recently by Sluijs et al. (2007a: 90 – 140 kyrs; see also Westerhold et al. 2009). Accumulation rates can be compared to those from the terrestrial record of the Bighorn Basin, USA (Sluijs et al. 2007a, Abdul Aziz et al. 2008), but are at least one magnitude larger than accumulation rates in pelagic sections, e.g., in the Belluno Basin

in northern Italy (DALLANAVE et al. 2009). By counting the sandy turbidites within this interval (240 layers) a periodicity of ca. 700 yrs (170 kyrs duration) can be reconstructed for turbidity currents entering the basin. The pronounced input of sand fraction is different from most other sections showing the Paleocene-Eocene transition (e.g. SCHMITZ & PUJALTE 2007) and can be interpreted as a result of regional tectonic activity overprinting the effects of global environmental perturbations.

Further constraints on the depositional environment of the Zwieselalm Formation in the Pichler section can be drawn from foraminiferal data. Agglutinated (arenaceous) foraminifera are rare in all samples investigated and small, size-sorted calcareous specimens dominate the assemblages if present. The frequency of foraminifera in the samples (individuals per gram dry sediment, right column of Table 1) may therefore be used as a rough indicator for the intensity of the dissolution of calcareous material (position of the CCD relative to the depositional depth) in the turbiditic depositional environment. Only a few foraminifera or a lack of foraminifera are recognized in the lower part of the section and an increase in the upper part (Tab. 2). The amount of (transported) foraminiferal tests is even higher above the assumingly autochthonous sample PEG-05 at 110.96 m. Following this line of evidence, sediments below section meter 62 (sample PEG-17) were therefore deposited clearly below CCD, those above 62 m close to the CCD, and samples PEG-03 to -05 probably above CCD. The depositional depth of the sediments in the lower part of the section was likely below 2.5 km if compared with depth ranges of the modern CCD (BERGER & WINTERER 1974), although a pronounced shallowing of the CCD across the PETM has been recognized (e.g. DICKENS et al. 1997).

The assemblage composition of sample PEG-36 at 10.30 m with *Trochamminoides* as the most frequent genus is more similar to the Late Cretaceous Krashenninikov Fauna as described in KAMINSKI et al. (1999) than the early Eocene Iberia-Celebes Fauna or assemblages of the *Glomospira*-acme (KAMINSKI 2005). Combined with high percentages of tubular, epifaunal suspension feeders (*Ammodiscus,* ?*Nothia, Psammosiphonella*) and a low infaunal content (*Reophax, Subreophax*), the assemblage shows the occupation of all ecologic niches, which may be interpreted as an indication for oligotrophic conditions at the sea bottom (KAMINSKI et al. 1999). This is supported by the presence of the very large *Arthodendron* fragments, a recently revised taxon (KAMINSKI et al. 2008). On the contrary the appearance of *Apectodinium* may indicate contemporaneously relatively nutrient-rich surface waters (CROUCH et al. 2001; SLUIJS & BRINKHUIS 2009).

The benthic assemblage of sample PEG-05 is dominated (70 %) by planconvex or biumbilicate epifaunal taxa (*Cibicidoides, Gavelinella, Hanzawaia*) and the infaunal, oxygen-deficiency tolerant taxa (*Aragonia, Bolivina, Bulimina*) is relatively low (21 %). Based on comparisons with modern and Paleogene faunas (e.g., BERNHARD 1986; MURRAY 1991; KAIHO 1991, 1994), oxic bottom waters with low nutrient supply can be assumed for this depositional interval.

Acknowledgements

Parwin Akrami, Sabine Giesswein and Helga Priewalder (all GBA, Vienna) are thanked for sample preparation and documentation. Ameer Elnady (University of Vienna) is thanked for lab work. Field work was supported by IGCP 555 and the Austrian Academy of Sciences. We thank A. Slujs for a critical review of the paper and Andreas Kroh for critical remarks and editorial work.

References

Abdul Aziz, H., Hilgen, F.J., van Luijk, G.M., Sluijs, A., Kraus, M.J., Pares, J.M. & Gingerich, P.D. (2008): Astronomical climate control on paleosol stacking patterns in the upper Paleocene – lower Eocene Willwood Formation, Bighorn Basin, Wyoming. – Geology, **36**: 531–534.

Aubry, M.-P. (1996): Towards an upper Paleocene-lower Eocene high resolution stratigraphy based on calcareous nannofiossil stratigraphy. – Israel Journal of Earth Sciences, **44**: 239–253.

Bernhard, J.M. (1986): Characteristic assemblages and morphologies of benthic foraminifera from anoxic, organic-rich deposits: Jurassic through Holocene. – Journal of Foraminiferal Research, **16**/3: 207–215.

Berger, W.H. & Winterer, E.L. (1974): Plate stratigraphy and the fluctuating carbonate line. – In: Hsü, K. & Jenkyns, H.C. (eds): Pelagic sediments on land and under the sea. – pp. 11–48, Oxford (Blackwell).

Berggren, W.A. & Pearson, P.N. (2005): A revised tropical to subtropical Paleogene planktonic foraminiferal zonation. – Journal of Foraminiferal Research, **35**: 279–298.

——, Kent, D.V., Swisher, C.C. & Aubry, M.-P. (1995): A revised Cenozoic geochronology and chronostratigraphy. – SEPM (Society for Sedimentary Geology) Special Publications, **54**: 129–212.

Bowen, G.J., Clyde, W.C., Koch, P.L., Ting, S., Alroy, J., Tsubamoto, T., Wang, Y. & Wang, Y. (2002): Mammalian dispersal at the Paleocene/Eocene boundary. – Science, **295**: 2062–2065.

Bown, P.R. (2005): Palaeogene calcareous nannofossils from the Kilwa and Lindi areas of coastal Tanzania (Tanzania Drilling Project 2003–4). – Journal of Nannoplankton Research, **27**: 21–95.

Bralower, t.J. (2002): Evidence of surface water oligotrophy during the Paleocene-Eocene thermal maximum: Nannofossil assemblage data from Ocean Drilling Program Site 690, Maud Rise, Weddell Sea. – Paleoceanography, **17**, doi: 10.1029/2001PA000662.

Bybell, L.M. & Self-Trail, J.M. (1994): Evolutionary, biostratigraphic, and taxonomic study of calcareous nannofossils from a continuous Paleocene–Eocene boundary section in New Jersey. – U.S. Geological Survey Professional Papers, **1554**: 1–107.

Crouch, E. M., Heilmann-Clausen, C., Brinkhuis, H., Morgans, H.E.G., Rogers, K.M., Egger, H. & Schmitz, B. (2001): Global dinoflagellate event associated with the Late Paleocene Thermal Maximum. – Geology, **29**: 315–318.

Dallanave, E., Agnini, C., Muttoni, G. & Rio, D. (2009): Magneto-biostratigraphy of the Cicogna section (Italy): Implications for the late Paleocene–early Eocene time scale. – Earth and Planetary Science Letters, **285**: 39–51.

DICKENS, G.R. (2004): Hydrocarbon-driven warming. – Nature, **429**: 513–515.

——, CASTILLO, M.M. & WALKER, J.C.G. (1997): A blast of gas in the latest Paleocene: Simulating first-order effects of massive dissociation of oceanic methane hydrate. – Geology, **25**: 259–262.

——, O´NEIL, J.R., REA, D.K. & OWEN, R.M. (1995): Dissociation of oceanic methane hydrate as a cause of the carbon isotope excursion at the end of the Palaeocene. – Paleoceanography, **10**: 965–971.

EGGER, H., FENNER, J., HEILMANN-CLAUSEN, C., RÖGL, F. SACHSENHOFER, R.F. & SCHMITZ, B. (2003): Paleoproductivity of the northwestern Tethyan margin (Anthering Section, Austria) across the Paleocene-Eocene transition. – In: WING, S.L., GINGERICH, P., SCHMITZ, B. & THOMAS, E. (eds): Causes and Consequences of Globally Warm Climates in the Early Paleogene. – Geological Society of America Special Paper, **369**: 133–146.

——, HEILMANN-CLAUSEN, C., SCHMITZ, B. (2000): The Paleocene/Eocene-boundary interval of a Tethyan deep-sea section and its correlation with the North Sea Basin. – Société Géologique de France Bulletin, **171**: 207–216.

——, HEILMANN-CLAUSEN, C. & SCHMITZ, B. (2009a): From shelf to abyss: Record of the Paleocene/Eocene-boundary in the Eastern Alps (Austria). – Geologica Acta, **7**: 215–227.

——, HOMAYOUN, M., HUBER, H., RÖGL, F. & SCHMITZ, B. (2005): Early Eocene climatic, volcanic, and biotic events in the northwestern Tethyan Untersberg section, Austria. – Palaeogeography, Palaeoclimatology, Palaeoecology, **217**: 243–264.

——, KOEBERL, C., SPÖTL, C., WAGREICH, M. & MOHAMED, O. (2009b): Paleogene deep-water deposits at Gams (Austria): From the K/Pg-boundary to the P/E-boundary in a Tethyan setting. – In: CROUCH, E.M., STRONG, C.P., HOLLIS, C.J. (eds): Climatic and Biotic Events of the Paleogene (CBEP 2009), extended abstracts volume, pp. 49–52.

——, RÖGL, F. & WAGREICH, M. (2004): Biostratigraphy and facies of Paleogene deep-water deposits at Gams (Gosau Group, Austria). – Annalen des Naturhistorischen Museums Wien, Serie A, **106**: 281–307.

—— & WAGREICH, M. (2001): Upper Paleocene – Lower Eocene nannofossils from the Gosau Group of Gams/Styria (Austria). – In: PILLER, W.E. & RASSER, M.W. (eds): Paleogene of the Eastern Alps. – Österreichische Akademie der Wissenschaften, Schriftenreihe der Erdwissenschaftlichen Kommissionen, **14**: 465–472.

GEROCH, S. & NOWAK, W. (1983): Proposal of zonation for the Late Tithonian – Late Eocene, based upon arenaceous foraminifera from the Outer Carpathians, Poland. – Benthos ‘83; 2nd International Symposium on Benthic Foraminifera (Pau, April 1983), pp. 225–239, Pau.

GIBBS, S.J., BOWN, P.R., SESSA, J.A., BRALOWER, T.J. & WILSON, P.A. (2006): Nannoplankton Extinction and Origination across the Paleocene-Eocene Thermal Maximum. – Science, **314** (5806): 1770–1773.

GINGERICH, P.D. (2006): Environment and evolution through the Paleocene-Eocene thermal maximum. – Trends in Ecology & Evolution, **21**: 246–253.

GRACHEV, A.F. (ed.) (2009): The K/T boundary of Gams (Eastern Alps, Austria) and the nature of terminal Cretaceous mass extinction. – Abhandlungen der Geologischen Bundesanstalt, **63**: 1–199.

——, Korchagin, O.A., Kollmann, H.A., Pechersky, D.M. & Tselmovich, A. (2005): A new look at the nature of the transitional layer at the K/T boundary near Gams, Eastern Alps, Austria, and the problem of the mass extinction of the biota. – Russian Journal of Earth Sciences, **7**: 1–45.

——, Korchagin, O.A., Tselmovich, V.A. & Kollmann, H.A. (2008): Cosmic dust and micrometeorites in the transitional clay layer at the Cretaceous-Paleogene boundary in the Gams Section. – Physics of the Solid Earth, **44**, 555–569.

Kaiho, K. (1991): Global changes of Paleogene aerobic/anaerobic benthic foraminifera and deep-sea circulation. – Palaeogeography, Palaeoclimatology, Palaeoecology, **83**: 65–85.

—— (1994): Benthic foraminiferal dissolved-oxygen index and dissolved-oxygen levels in the modern ocean. – Geology, **22**: 719–722.

Kaminski, M. A. (2005): The utility of deep-water agglutinated foraminiferal acmes for correlating Eocene to Oligocene abyssal sediments in the North Atlantic and Western Tethys. – In: Tyska, J., Oliwkiewicz-Miklasinska, M., Gedl, P. & Kaminski, M.A. (eds): Methods and Applications in Micropaleontology, **124**: 325–339.

——, Kuhnt W. & Moullade M. (1999): The evolution and paleobiogeography of abyssal agglutinated foraminifera since the Early Cretaceous: A tale of four faunas. – Neues Jahrbuch für Geologie und Paläontologie, Abhandlungen, **212**/1–3: 401–439.

——, Uchman, A., Neagu, T. & Cetean, C.G. (2008): A larger agglutinated foraminifera originally described as a marine plant: the case of *Arthrodendron* Ulrich, 1904 (Foraminifera), its synonyms and homonyms. – Journal of Micropaleontology, **27**: 103–110.

Kelly, D.C., Bralower, T.J. & Zachos, J.C. (1998): Evolutionary consequences of the latest Paleocene thermal maximum for tropical planktonic foraminifera. – Palaeogeography, Palaeoclimatology, Palaeoecology, **141**: 139–161.

——, Bralower, T.J., Zachos, J.C., Premoli Silva, I. & Thomas, E. (1996): Rapid diversification of planktonic foraminifera in the tropical Pacific (ODP Site 865) during the late Paleocene thermal maximum. – Geology, **24**: 423–426.

Kent, D.V., Cramer, B.S., Lanci, L., Wang, D., Wright, J.D. & Van der Voo, R. (2003): A case for a comet impact trigger for the Paleocene/Eocene thermal maximum and carbon isotope excursion. – Earth and Planetary Science Letters, **211**: 13–26.

Kollmann, H.A. (1963): Zur stratigraphischen Gliederung der Gosauschichten von Gams. – Mitteilungen der Gesellschaft der Geologie- und Bergbaustudenten, **13**: 189–212.

—— (1964): Stratigraphie und Tektonik des Gosaubeckens von Gams (Steiermark, Österreich). – Jahrbuch der Geologischen Bundesanstalt, **107**: 71–159.

Kopp, R.E., Raub, T.D., Schumann, D., Vali, H., Smirnov, A.V. & Kirschvink, J.L. (2007): Magnetofossil spike during the Paleocene-Eocene thermal maximum: Ferromagnetic resonance, rock magnetic, and electron microscopy evidence from Ancora, New Jersey, United States. – Paleoceanography, **22**: PA4103, doi:10.1029/2007PA001473.

Kurtz, A., Kump, L.R., Arthur, M.A., Zachos, J.C. & Paytan, A. (2003): Early Cenozoic decoupling of the global carbon and sulfur cycles. – Paleoceanography, **18**: 1090, doi:10.1029/2003PA000908.

Laenen, B & De Craen, M. (2004): Eogenetic siderite as an indicator for fluctuations in sedimentation rate in the Oligocene Boom Clay Formation (Belgium). – Sedimentary Geology, **163**: 165–174.

LAHODYNSKY, R. (1988a): Lithostratigraphy and sedimentology across the Cretaceous/Tertiary boundary in the Flyschgosau (Eastern Alps, Austria). – Revista Espanola Paleontologia Extraordinaro, **1988**: 73–82.

—— (1988b): Geology of the K/T boundary site at Knappengraben creek (Gams, Styria). – IGCP Project 199 "Rare events in geology"; Abstracts. – Berichte der Geologischen Bundesanstalt, **15**: 33–36.

LIPPERT, P.C. & ZACHOS, J.C. (2007): A biogenic origin for anomalous fine-grained magnetic material at the Paleocene-Eocene boundary at Wilson Lake, New Jersey. – Paleoceanography, **22**: PA4104, doi:10.1029/2007PA001471.

LU, G. & KELLER, G. (1993): The Palaeocene–Eocene transition in the Antartic Indian Ocean: Inference from planktic foraminifera. – Marine Micropalaeontology, **21**: 101–142.

LUTERBACHER, H.P., HARDENBOL, J. & SCHMITZ, B. (2000): Decision of the voting members of the International Subcommission on Paleogene Stratigraphy on the criterion of recognition of the Paleocene/Eocene–boundary. – Newsletter of the International Subcommission on Paleogene Stratigraphy, **9**: 13.

MARTINI, E. (1971): Standard Tertiary and Quaternary calcareous nannoplankton zonation. – In: FARINACCHI, A. (ed.): Proceedings II Planktonic Conference Roma 1970/2, pp.739–785.

MURRAY, J.W. (1991): Ecology and palaeoecology of benthic foraminifera. – 397 p., Harlow (Longman Scientific & Technical).

MURPHY, B.H., FARLEY, K.A. & ZACHOS, J.C. (2010): An extraterrestrial 3He-based timescale for the Paleocene-Eocene thermal maximum (PETM) from Walvis Ridge, IODP Site 1266. – Geochimica Et Cosmochimica Acta, **74**: 5098–5108.

OLSSON R. K., HEMLEBEN C., BERGGREN W. A. & HUBER B. T. (1999): Atlas of Paleocene planktonic foraminifera. – Smithonian Contributions to Paleobiology, **85**: 1–252.

PANCHUK, K., RIDGWELL, A. & KUMP, L.R. (2008): Sedimentary response to Paleocene-Eocene Thermal Maximum carbon release: A model-data comparison. – Geology, **36**: 315–318.

PEARSON P. N., OLSSON R. K., HUBER B. T., HEMLEBEN C., BERGGREN W. A. & COXALL H. K. (2006): Overview of Eocene planktonic foraminiferal taxonomy, paleoecology, phylogeny, and biostratigraphy. – In: PEARSON, P.N., OLSSON, R.K., HUBER, B.T., HEMLEBEN, C. & BERGGREN, W.A. (eds.): Atlas of Eocene planktonic foraminifera. – Cushman Foundation Special Publication **41**: 11–28.

PICKERING, K.T., HISCOTT, R.N. & HEIN, F.J. (1989): Deep-marine environments. 416 p., London (Unwin Hyman).

RAFFI, I., BACKMAN, J., ZACHOS, J.C. & SLUIJS, A. (2009): The response of calcareous nannofossil assemblages to the Paleocene Eocene Thermal Maximum at the Walvis Ridge in the South Atlantic. – Marine Micropaleontology, **70**: 201–212.

RÖHL, U., BRALOWER, T.J., NORRIS, R.D. & WEFER, G., (2000): New chronology for the late Palaeocene thermal maximum and its environmental implications. – Geology, **28**: 927–930.

——, WESTERHOLD, T., BRALOWER, T.J. & ZACHOS, J.C. (2007): On the duration of the Paleocene – Eocene thermal maximum (PETM). – Geochemistry, Geophysics, Geosystems, **8**: Q12002, doi:10.1029/2007GC001784.

SCHMITZ, B. & PUJALTE, V. (2007): Abrupt increase in extreme seasonal precipitation at the Paleocene-Eocene boundary. – Geology, **35**: 215–218.

Sluijs, A. & Brinkhuis, H. (2009): A dynamic climate state during the Paleocene-Eocene Thermal Maximum: inferences from dinoflagellate cyst assemblages on the New Jersey Shelf. – Biogeosciences, **6**: 1755–1781.

—, Brinkhuis, H., Crouch, E.M. et al. (2008): Eustatic variations during the Paleocene-Eocene greenhouse world. – Paleoceanography, **23**: PA4216.

—, Brinkhuis, H., Schouten, S., Bohaty, S.M., John, C.M., Zachos, J.C., Sinninghe Damsté, J.S., Crouch, E.M. & Dickens, G.R. (2007b): Environmental precursors to light carbon input at the Paleocene/Eocene boundary. – Nature, **450**: 1218–1221.

—, Bowen, G.J., Brinkhuis, H., Lourens, L.J. & Thomas, E. (2007a): The Palaeocene-Eocene Thermal Maximum super greenhouse: biotic and geochemical signatures, age models and mechanisms of global change. – In: Williams, M., Haywood, A.M., Gregory, J. & Schmidt, D.N. (eds.): Deep-Time Perspectives on Climate Change: Marrying the Signal from Computer Models and Biological Proxies. The Micropalaeontological Society, Special Publications. – pp. 323–349, London (Geological Society London).

—, Schouten, S., Pagani, M. et al. (2006): Subtropical Arctic Ocean temperatures during the Palaeocene/Eocene thermal maximum. – Nature, **441**: 610–613.

Spötl, C. & Vennemann, T. (2003): Continuous-flow IRMS analysis of carbonate minerals. – Rapid Communications in Mass Spectrometry, **17**:1004–1006.

Stradner, H. & Rögl, F. (1988): Microfauna and nannoflora of the Knappengraben section (Austria) across the Cretaceous/Tertiary boundary. IGCP Proj. 199 „Rare events in geology", Abstracts. – Berichte der Geologischen Bundesanstalt, **15**: 25–26.

Summesberger, H. & Kennedy, W. J. (1996): Turonian ammonites from the Gosau Group (Upper Cretaceous; Northern Calcareous Alps, Austria), with a revision of *Barroisiceras haberfellneri* (HAUER, 1866). – Beiträge zur Paläontologie Österreichs, **21**: 105–177.

—, Wagreich, M. & Bryda, G. (2009): Upper Maastrichtian cephalopods and the correlation to calcareous nannoplankton and planktic foraminifera zones in the Gams Basin (Gosau Group; Styria, Austria). – Annalen des Naturhistorischen Museums Wien, Serie A, **111**: 159–182.

—, Wagreich, M., Tröger, K.-A. & Jagt, J.W.M. (1999): Integrated biostratigraphy of the Santonian/Campanian Gosau Group of the Gams area (Late Cretaceous; Styria, Austria). – Beiträge zur Paläontologie Österreichs, **24**: 155–205.

Svensen, H., Planke, S., Malthe-Sorenssen, A., Jamtveit, B., Myklebust, R., Rasmussen Eidem, T. & Rey, S.S. (2004): Release of methane from a volcanic basin as a mechanism for initial Eocene global warming. – Nature, **429**: 542–545.

Thomas, E. (1998): Biogeography of the Late Paleocene benthic foraminiferal extinction.– In: Aubry, M.–P., Lucas, S. & Berggren, W.A. (eds.): Late Paleocene-Early Eocene climatic and biotic events in the marine and terrestrial records. – pp. 214–243, New York (Columbia University Press).

— (2007): Cenozoic mass extinctions in the deep sea: what perturbs the largest habitat on earth? – Geological Society of America Special Paper, **424**: 1–24.

Tjalsma, R.C. & Lohmann, G.P. (1983): Paleocene-Eocene bathyal and abyssal benthic foraminifera from the Atlantic Ocean. – Micropaleontology Special Publication, **4**: 1–90.

Tremolada, F. & Bralower, T.J. (2004): Nannofossil assemblage fluctuations during the Paleocene-Eocene Thermal Maximum at Sites 213 (Indian Ocean) and 401 (North Atlantic Ocean): palaeoocenaographic implications. – Marine Micropaleontology, **52**: 107–116.

WAGREICH, M. (1993): Subcrustal tectonic erosion in orogenic belts – A model for the Late Cretaceous subsidence of the Northern Calcareous Alps (Austria). – Geology, **21**: 941–944.

—— (2001): Paleocene – Eocene paleogeography of the Northern Calcareous Alps (Gosau Group, Austria). – In: PILLER, W.E. & RASSER, M.W. (Eds): Paleogene of the Eastern Alps. – Österreichische Akademie der Wissenschaften, Schriftenreihe der Erdwissenschaftlichen Kommissionen, **14**: 57–75.

——(2004): Biostratigraphy and lithostratigraphy of the Krimpenbach Formation (Upper Santonian – Campanian), Gosau Group of Gams (Austria). – Annalen des Naturhistorischen Museums Wien, Serie A, **106**: 123–138.

—— (ed.) (2009): Rapid Environmental/Climate Changes and Catastrophic Events in Late Cretaceous and Early Paleogene. RECCCE Workshop Abstracts and Excursion Guide. – Berichte der Geologischen Bundesanstalt, **78**: 74 pp.

—— & FAUPL, P. (1994): Palaeogeography and geodynamic evolution of the Gosau Group of the Northern Calcareous Alps (Late Cretaceous, Eastern Alps, Austria). – Palaeogeography, Palaeoclimatology, Palaeoecology, **110**: 235–254.

—— & KRENMAYR, H.-G. (1993): Nannofossil biostratigraphy of the Late Cretaceous Nierental Formation, Northern Calcareous Alps (Bavaria, Austria). – Zitteliana, **20**: 67–77.

WALKER, R.G. (1978): Deep water sandstone facies and ancient submarine fans: models for exploration of stratigraphic traps. – AAPG Bulletin, **62**: 932–966.

WESTERHOLD, T., RÖHL, U., MCCARREN, H.K. & ZACHOS, J.C. (2009): Latest on the absolute age of the Paleocene–Eocene Thermal Maximum (PETM): New insights from exact stratigraphic position of key ash layers + 19 and – 17. – Earth and Planetary Science Letters, **287**: 412–419.

WICHER, C.A. (1956): Die Gosau-Schichten im Becken von Gams (Österreich) und die Foraminiferengliederung der höheren Oberkreide in der Tethys. – Paläontologische Zeitschrift, **30**: 87–136.

WING, S. L, BOWN, T.M. & OBRADOVIC, J. D. (1991): Early Eocene biotic and climatic change in interior western North America. – Geology, **19**: 1189–1192.

WOOD, G.D., GABRIEL, A.M. & LAWSON, J.C. (1996): Palynological techniques: processing and microscopy. – In: JANSONIUS, J. & MCGREGOR, D.C. (eds): Palynology: Principles and Applications (Vol. 1). American Association Stratigraphical Palynology Foundation, pp. 29–50.

ZACHOS, J.C., BOHATY, S.M., JOHN, C.M., MCCARREN, H., KELLY, C.C. & NIELSEN, T. (2007): The Palaeocene-Eocene carbon isotope excursion: constraints from individual shell planktonic foraminifer records. – Philosopical Transactions of the Royal Society A, **365**: 1829–1842.

——, RÖHL, U., SCHELLENBERG, S.A., et al. (2005): Rapid Acidification of the Ocean during the Paleocene-Eocene Thermal Maximum. – Science, **308**: 1611–1615.

Plate 1

Agglutinated foraminifera

Figs 1, 2, 8: *Arthrodendron diffusum* (Ulrich, 1904)

Fig. 3: ?*Nothi*a sp.

Fig. 4: *Psammosiphonella cylindrica* (Glaessner, 1937)

Fig. 5: *Ammodiscus glabratus* Cushman & Jarvis, 1928

Fig. 6: *Psammosphaera fusca* Schulze, 1875

Fig. 7: *Placentammina placenta* (Grzybowski, 1898)

Fig. 9: *Ammodiscus siliceus* (Terquem, 1862)

Fig. 10: *Glomospirella gaultina* (Berthelin, 1880)

Fig. 11: "*Glomospira*" irregularis (Grzybowski, 1898)

Fig. 12: *Dolgenia* sp.

Fig. 13: *Kalamopsis grzybowskii* (Dylasanka, 1923)

Fig. 14: *Hyperammina* cf. *nuda* Subbotina, 1950

Fig. 15: *Reophax duplex* Grzybowski, 1896

Fig. 16: *Subreophax* sp.

Fig. 17: *Reophax* cf. *minuta* Tappan, 1940

Fig. 18: *Hormosina velascoensis* (Cushman, 1926)

Fig. 19: *Reophax subnodulosus* Grzybowski, 1898

Fig. 20: *Trochammina* sp.

Fig. 21: *Trochamminoides dubius* (Grzybowski, 1901)

Fig. 22: *Recurvoides* sp.

Figs 23, 24: *Thalmannammina subturbinata* (Grzybowski, 1898)

Fig. 25: *Trochamminoides proteus* (Karrer, 1866)

Fig. 26: *Trochamminoides variolarius* (Grzybowski, 1898)

All from sample PEG 36, length of scale bars 0.1 mm.

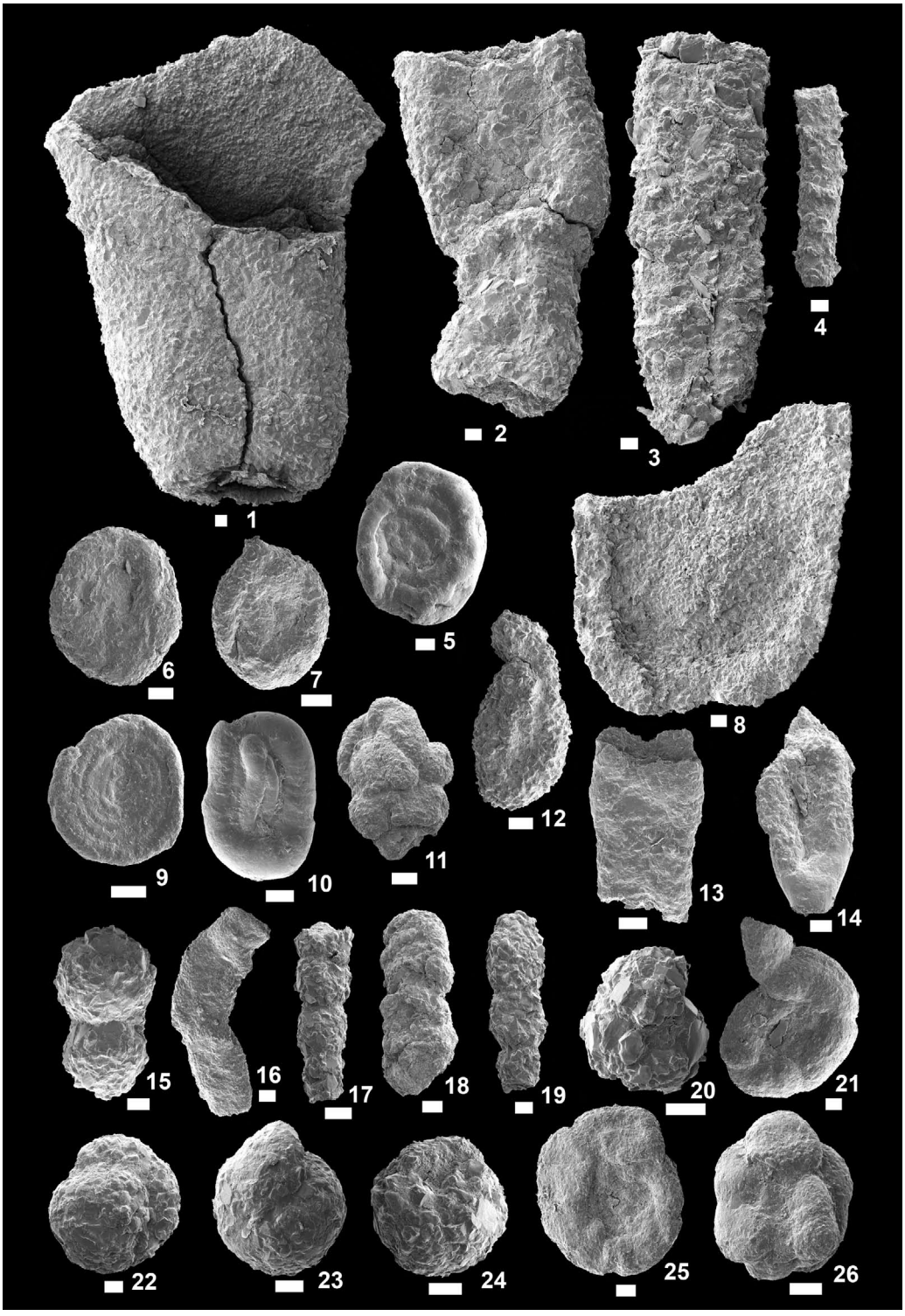
1
2
3
4
5
6
7
8
9
10
11
12
13
14
15
16
17
18
19
20
21
22
23
24
25
26

Plate 2

Planktic and calcareous benthic foraminifera

Fig. 1: *Acarinina coalingensis* (Cushman & Hanna, 1927)

Fig. 2: *Acarinina* cf. *esnaensis* (LeRoy, 1953)

Fig. 3: *Acarinina nitida* (Martin, 1943)

Fig. 4: *Acarinina soldadoensis* (Brönnimann, 1952)

Fig. 5: *Acarinina subsphaerica* (Subbotina, 1947)

Fig. 6: *Morozovella acuta* (Toulmin, 1941)

Fig. 7: *Morozovella aequa* (Cushman & Renz, 1942)

Fig. 8: *Morozovella apanthesma* (Loeblich & Tappan, 1957)

Fig. 9: *Morozovella gracilis* (Bolli, 1957)

Fig. 10: *Morozovella occlusa* (Loeblich & Tappan, 1957)

Fig. 11: *Morozovella subbotinae* (Morozova, 1939)

Fig. 12: *Parasubbotina varianta* (Subbotina, 1953)

Fig. 13: *Planorotalites pseudoscitula* (Glaessner, 1937)

Fig. 14: *Subbotina triangularis* (White, 1928)

Fig. 15: *Chiloguembelina trinitatensis* (Cushman & Renz, 1942)

Fig. 16: *Aragonia velascoensis* (Cushman, 1925)

Fig. 17: *Bolivina midwayensis* Cushman, 1936

Fig. 18: *Bulimina* sp. (?cf. *bradbury* Martin, 1943)

Fig. 19: *Bulimina* cf. *trinitatensis* Cushman & Jarvis, 1928

Fig. 20: *Stilostomella gracillima* (Cushman, 1933)

Fig. 21: *Stilostomella subspinosa* (Cushman, 1943)

Figs 22, 23: *Cibicidoides tuxpamensis* (Cole, 1928)

Fig. 24: *Gavelinella danica* (Brotzen, 1940)

Fig. 25: *Gavelinella* cf. *micra* (Bermudez, 1949)

Fig. 26: *Hanzawaia cushmani* (Nuttall, 1930)

All from sample PEG 05, except 16 (PEG 04), length of scale bars 0.1 mm.

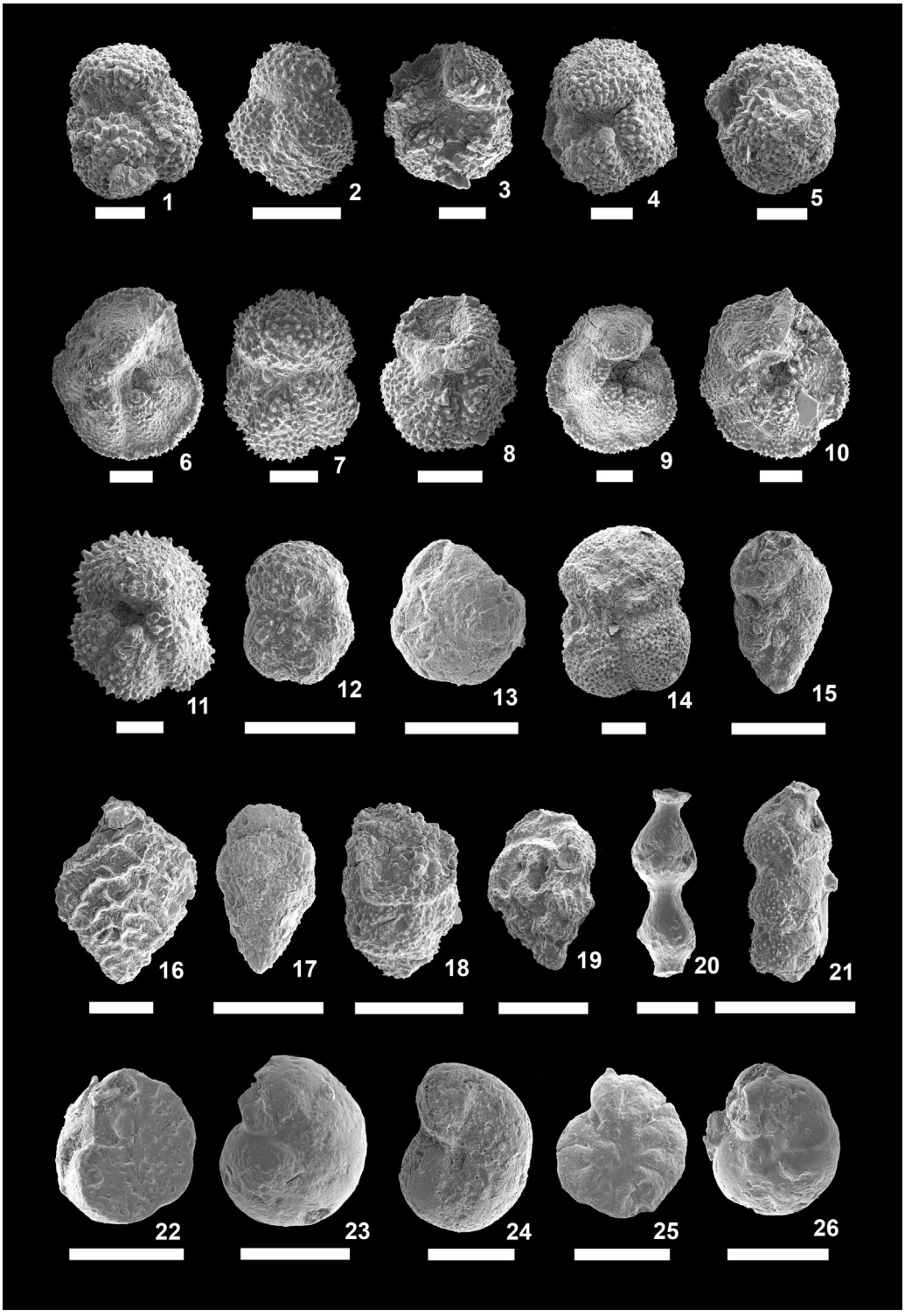
1
2
3
4
5
6
7
8
9
10
11
12
13
14
15
16
17
18
19
20
21
22
23
24
25
26